Supplementary Information:

Dynamical topology of chiral and nonreciprocal state transfers in a non-Hermitian quantum system

Pengfei Lu[1,2,5], Yang Liu[1,3,5], Qifeng Lao[1], Teng Liu[1], Xinxin Rao[1],
Ji Bian[1], Hao Wu[1], Feng Zhu[1,2,4], Le Luo[1,2,3,4,*]

[1]School of Physics and Astronomy, Sun Yat-sen University, Zhuhai 519082, China.

[2]Center of Quantum Information Technology,
Shenzhen Research Institute of Sun Yat-Sen University, Nanshan Shenzhen 518087, China.

[3]Quantum Science Center of Guangdong-HongKong-Macao Greater Bay Area,
Shenzhen 518048, China.

[4]Guangdong Provincial Key Laboratory of Quantum Metrology and Sensing,
Sun Yat-sen University, Zhuhai 519082, China.

[5]These authors contributed equally: Pengfei Lu, Yang Liu.

[*]Corresponding author. E-mail: luole5@mail.sysu.edu.cn

Supplementary Note 1: Time-varying nonadiabatic transition amplitude of $\mathcal{PT}$ Hamiltonian

The nonadiabatic transition amplitudes with a $\mathcal{PT}$-symmetric Hamiltonian have been measured in our experiments, as depicted in Fig. S1. The time-dependent amplitude coefficients of $C_1(t)$ and $C_2(t)$ are determined by $|\psi(t)\rangle = C_1(t)|\alpha(t)\rangle + C_2(t)|\beta(t)\rangle$. The crossing of $C_1(t)$ and $C_2(t)$ serves as a characterization of the nonadiabatic transition. According to stability loss delay, the time-varying relative nonadiabatic transition amplitude $R_1(t)$ and $R_2(t)$ can also be obtained by measuring $C_1(t)$ and $C_2(t)$, Specifically, these are given by $R_1(t) = \frac{C_2(t)}{C_1(t)}$ and $R_2(t) = \frac{C_1(t)}{C_2(t)}$, as discussed in the main text.

Supplementary Note 2: The winding number of the complex-energy bands

In this section, we explain that dynamic vorticity can be treated as the winding number of the complex-energy bands, and the singularity of complex-energy Riemann surface allows for the half-integer windings of the paired bands. It is important to note that the loop in Fig. 2a does not involve DNAT and has a winding number $\mathcal{V} = 1/2$. To calculate the winding number of a loop that involves DNATs, the evolution processes must be transformed into the parallel transported eigenbasis to obtain the dynamic vorticity as mentioned in the main text.

In this basis, loops involving DNATs can be parametrized by the encircling angle $\theta \in [0, 2\pi]$ around the EP. The theoretical results for θ in the complex-energy plane are shown in Fig. S2. The solid and dashed curves represent the theoretical loop and the projection of energy trajectories, respectively. Each band's dynamic vorticity $\mathcal{V}_\mathcal{D}$ is 1/2, which is the dynamic counterpart compared to the winding number of the stationary non-Hermitian band structures (*1*). The positive or negative value of the winding number depends on the orientation of encircling curve; it

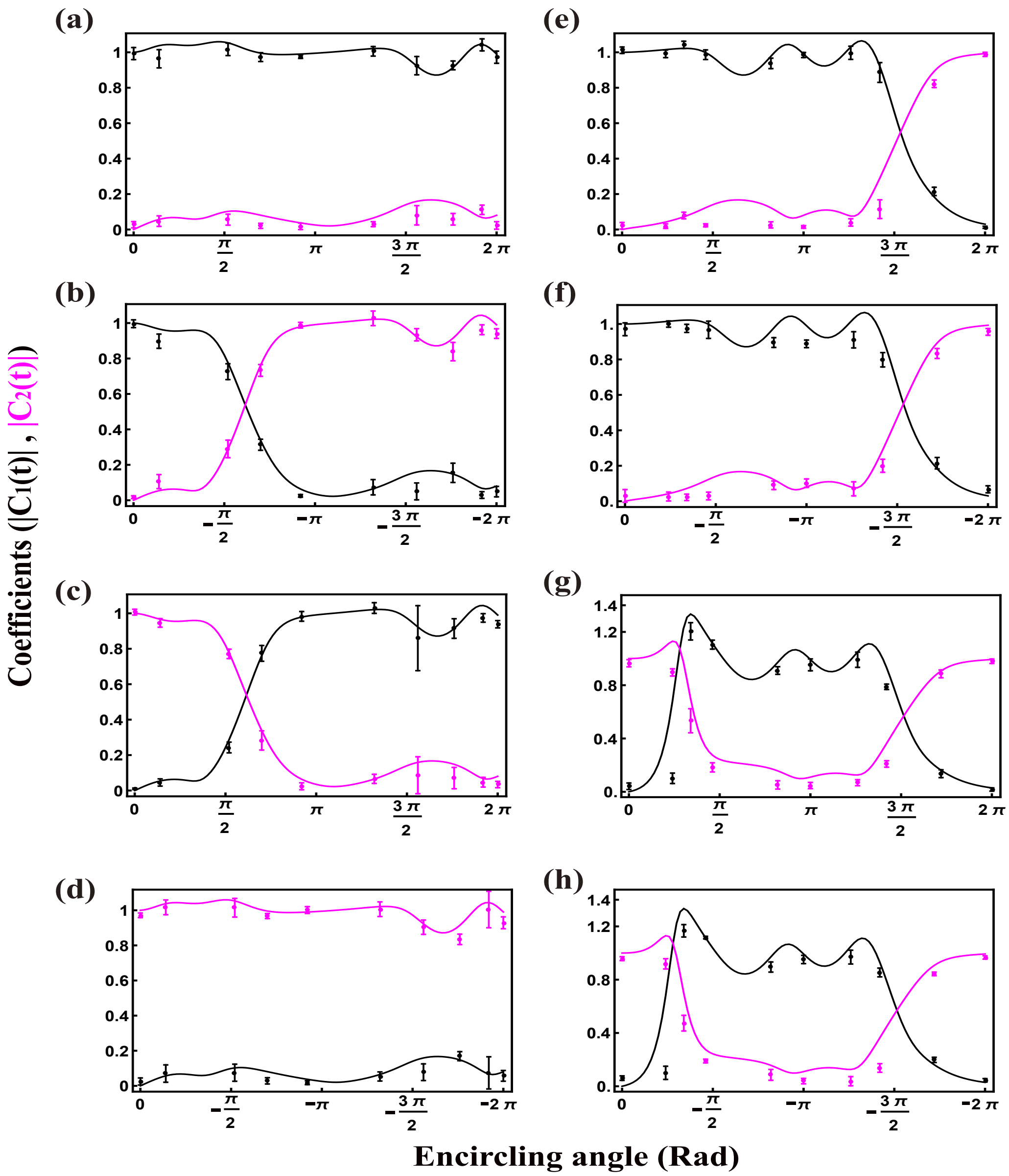

Figure S1: Amplitude coefficients of the instantaneous eigenstates when the $\mathcal{PT}$ Hamiltonian encircles the EP. (a-d) Encircling starting from the $\mathcal{PT}$-symmetric regime: (a) Clockwise with the initial state $|\alpha_A(0)\rangle$. (b) Counterclockwise with the initial state $|\alpha_A(0)\rangle$. (c) Clockwise with the initial state $|\beta_A(0)\rangle$. (d) Counterclockwise with the initial state $|\beta_A(0)\rangle$. (e-h) Encircling starting from the $\mathcal{PT}$-broken regime: (e) Clockwise with the initial state $|\alpha_B(0)\rangle$. (f) Counterclockwise with the initial state $|\alpha_B(0)\rangle$. (g) Clockwise with the initial state $|\beta_B(0)\rangle$. (h) Counterclockwise with the initial state $|\beta_B(0)\rangle$.

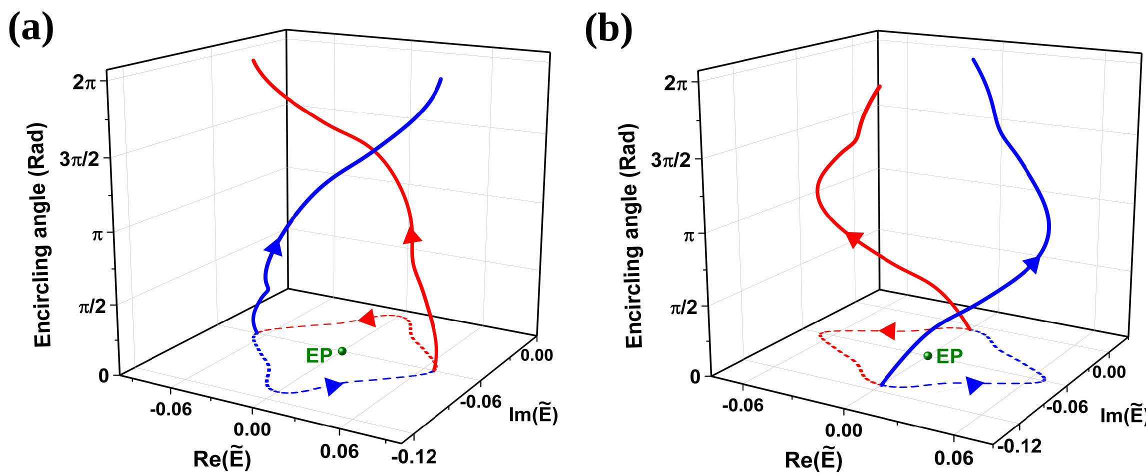

Figure S2: Windings of the complex-energy band structure in parallel transported basis. (a) The encirclement starting from the $\mathcal{PT}$-symmetric regime. (b) The encirclement starting from the $\mathcal{PT}$-broken regime. The encircling angle $\theta \in [0, 2\pi]$ parametrizes the closed loop, and dashed curves are the projection of the energy trajectory. The red and blue colors represent the different bands, and the olive circles represent the exceptional point (EP).

is negative if the curve travels around the EP in a clockwise direction.

Supplementary Note 3: Dynamically encircling of the $\mathcal{APT}$ Hamiltonian

The construction of the $\mathcal{APT}$-symmetric Hamiltonian has been demonstrated in our previous work (*2*). The evolution operator of the $\mathcal{APT}$ Hamiltonian $U(\tau) = e^{-iH'_{eff}t}$, is constructed by sandwiching a passive $\mathcal{PT}$-symmetric Hamiltonian H_{eff} between two $\pi/2$ pulses along the $\pm Y$ axis on the Bloch sphere. First, a $-\pi/2$ microwave pulse is applied along the Y axis in the rotating frame. Then, identical to the construction of the $\mathcal{PT}$-symmetric Hamiltonian, a microwave field along the X axis with strength J and a dissipation laser beam are applied simultaneously for a duration t. Finally, a $\pi/2$ pulse along the Y is implemented. The whole evolution is described as

$$R_y(\frac{\pi}{2})e^{-iH_{eff}t}R_y(-\frac{\pi}{2}) = e^{-iR_y(\frac{\pi}{2})H_{eff}R_y(-\frac{\pi}{2})t} = e^{-i(2i\gamma I_x - 2JI_z - i\gamma\mathbf{I})t} = e^{-iH'_{eff}t}, \tag{S1}$$

where the passive $\mathcal{APT}$-symmetric Hamiltonian is

$$H'_{eff} = \begin{pmatrix} -J - i\gamma & i\gamma \\ i\gamma & J - i\gamma \end{pmatrix}. \tag{S2}$$

It differs from the $\mathcal{APT}$-symmetric Hamiltonian

$$H_{APT} = \begin{pmatrix} -J & i\gamma \\ i\gamma & J \end{pmatrix}. \tag{S3}$$

by a term $i\gamma\mathbf{I}$. H_{APT} satisfies the anti-commutation relation $\{H_{\mathcal{APT}}, \mathcal{PT}\} = 0$ and is a pseudo-Hermitian (*3*), satisfying $\sigma_z^{-1}H_{\mathcal{APT}}\sigma_z = H^{\dagger}_{\mathcal{APT}}$.

The experimental timing sequence of dynamically encircling the EP of the $\mathcal{APT}$-symmetric Hamiltonian is shown in Fig. S3. Here, the Riemann surfaces defined by $\{\frac{J}{\gamma}, \frac{\Delta}{\gamma}, Re[\lambda]\}$ and $\{\frac{J}{\gamma}, \frac{\Delta}{\gamma}, Im[\lambda]\}$ are identical to those of the $\mathcal{PT}$-symmetric Hamiltonian due to the same complex eigenvalues.

Fig. S4 shows the state evolution when the initial states of encircling are in the $\mathcal{PTS}$ regime of $\mathcal{APT}$ symmetric Hamiltonian, where the nonreciprocal state transfer can be observed. For

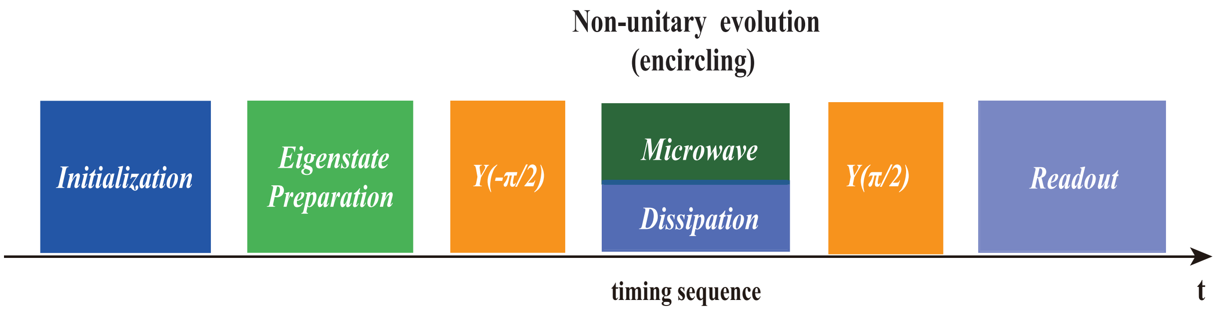

Figure S3: The timing sequence of the coupling microwave and dissipation laser for realizing the dynamical encircling of the EP with the $\mathcal{APT}$-symmetric Hamiltonian. $Y(\pm\pi/2)$ denotes the rotation along the $\pm Y$ axis by $\pi/2$ pulse.

example, the forward-time evolution $|\beta'_A(0)\rangle \xrightarrow{\text{CW}} |\alpha'_A(0)\rangle$ (trajectory 7′) and its backward-time evolution $|\alpha'_A(0)\rangle \xrightarrow{\text{CCW}} |\alpha'_A(0)\rangle$ (trajectory 6′) illustrate this nonreciprocal behavior. Similarly, the forward-time evolution $|\beta'_A(0)\rangle \xrightarrow{\text{CCW}} |\alpha'_A(0)\rangle$ (trajectory 8′) and its backward-time evolution $|\alpha'_A(0)\rangle \xrightarrow{\text{CW}} |\alpha'_A(0)\rangle$ (trajectory 5′) further exemplify this nonreciprocal behavior.

Fig. S5 shows the state evolution when the initial state of encircling is in the $\mathcal{PTB}$ regime of the $\mathcal{APT}$ symmetric Hamiltonian, where both the chiral and nonreciprocal state transfer can be observed. The clockwise evolution $|\alpha'_B(0)\rangle \xrightarrow{\text{CW}} |\beta'_B(0)\rangle$ (trajectory 1′) and counterclockwise evolution $|\alpha'_B(0)\rangle \xrightarrow{\text{CCW}} |\alpha'_B(0)\rangle$ (trajectory 2′) exhibit the chiral behavior, similar to trajectory 3′ $|\beta'_B(0)\rangle \xrightarrow{\text{CW}} |\beta'_B(0)\rangle$ and trajectory 4′ $|\beta'_B(0)\rangle \xrightarrow{\text{CCW}} |\alpha'_B(0)\rangle$. Nonreciprocal state transfer is also illustrated in the pair of the forward-time evolution $|\alpha'_B(0)\rangle \xrightarrow{\text{CCW}} |\alpha'_B(0)\rangle$ (trajectory 2′) and the backward-time evolution $|\alpha'_B(0)\rangle \xrightarrow{\text{CW}} |\beta'_B(0)\rangle$ (trajectory 1′), as well as in the pair of trajectory 3′ $|\beta'_B(0)\rangle \xrightarrow{\text{CW}} |\beta'_B(0)\rangle$ and trajectory 4′ $|\beta'_B(0)\rangle \xrightarrow{\text{CCW}} |\alpha'_B(0)\rangle$.

It is noticed that the chiral and nonreciprocal dynamics of the $\mathcal{PTB}$ regime of the $\mathcal{APT}$ symmetric Hamiltonian are analogous to those in the $\mathcal{PTS}$ regime of the $\mathcal{PT}$ symmetric Hamiltonian, and vice versa. We summarize the chiral, nonchiral, reciprocal, and nonreciprocal behaviors of both $\mathcal{PT}$ and $\mathcal{APT}$ symmetric Hamiltonians in Table. S1.

The experimental results of DNATs for the $\mathcal{APT}$-symmetric Hamiltonian are shown in

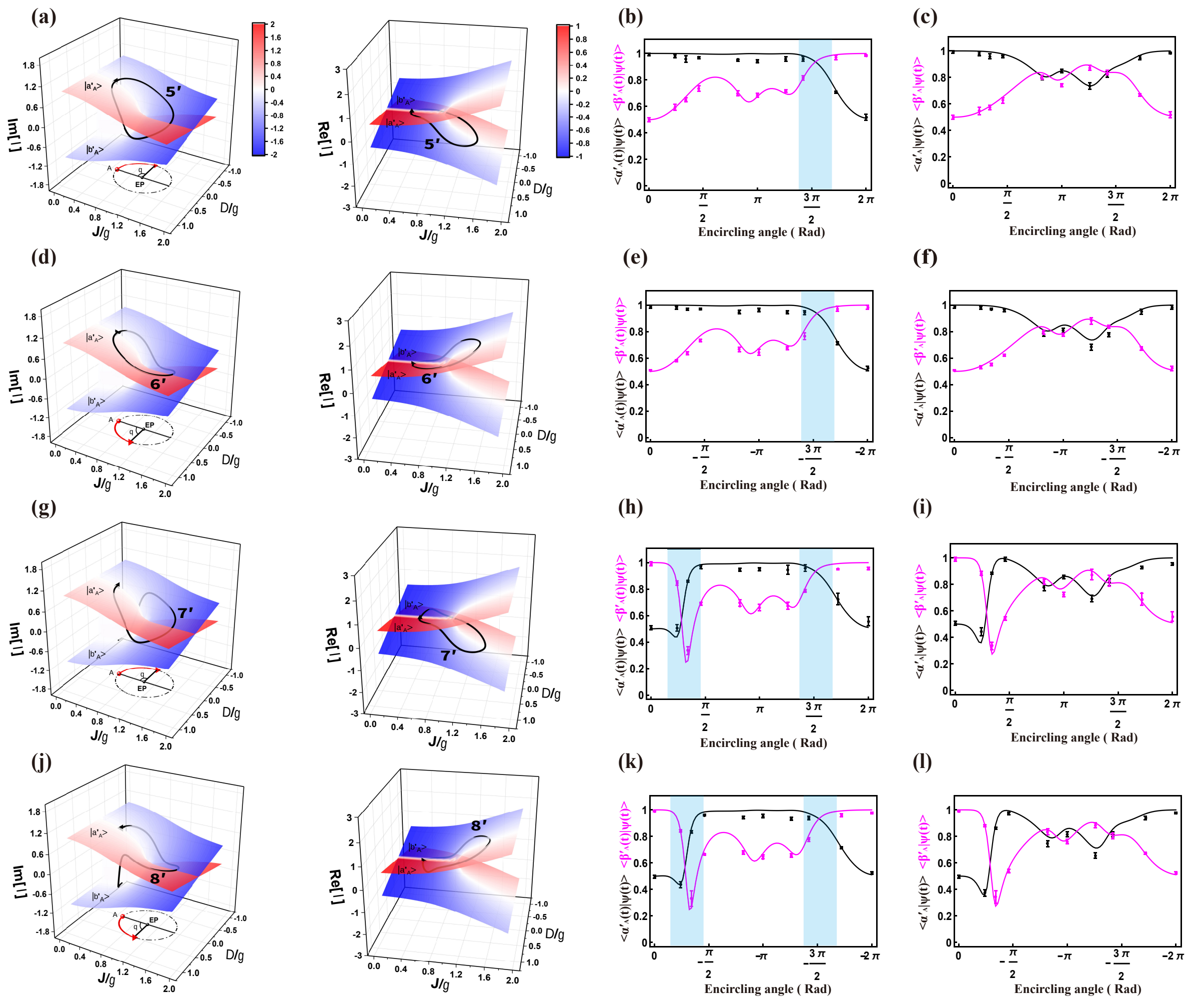

Figure S4: Time evolution of $|\psi(t)\rangle$ starting from the $\mathcal{PTS}$ regime of the $\mathcal{APT}$ symmetric Hamiltonian. The first two columns (a, d, g, and j) depict the trajectories of the state evolution on the eigenvalue Riemann surface. The third column (b, e, h, and k) depicts the overlap between the evolutionary state and two time-dependent eigenstates $\langle\alpha'_A(t)|\psi(t)\rangle$ and $\langle\beta'_A(t)|\psi(t)\rangle$, where the cyan shaded regions indicate the occurrence of nonadiabatic dynamics. The fourth column (c, f, i, and l) represents the overlap between the evolutionary state and two initial eigenstates. (a–c) Clockwise encircling with the initial state $|\alpha'_A(0)\rangle$. (d–f) Counterclockwise encircling with the initial state $|\alpha'_A(0)\rangle$. (g–i) Clockwise encircling with the initial state $|\beta'_A(0)\rangle$. (j–l) Counterclockwise encircling with the initial state $|\beta'_A(0)\rangle$. Circles and lines represent experimental measurements and numerical simulations, respectively.

Fig. S6 and S7. The notation and procedure are similar to those used in the experiments for measuring DNATs for the $\mathcal{PT}$-symmetric Hamiltonian as described in the main text.

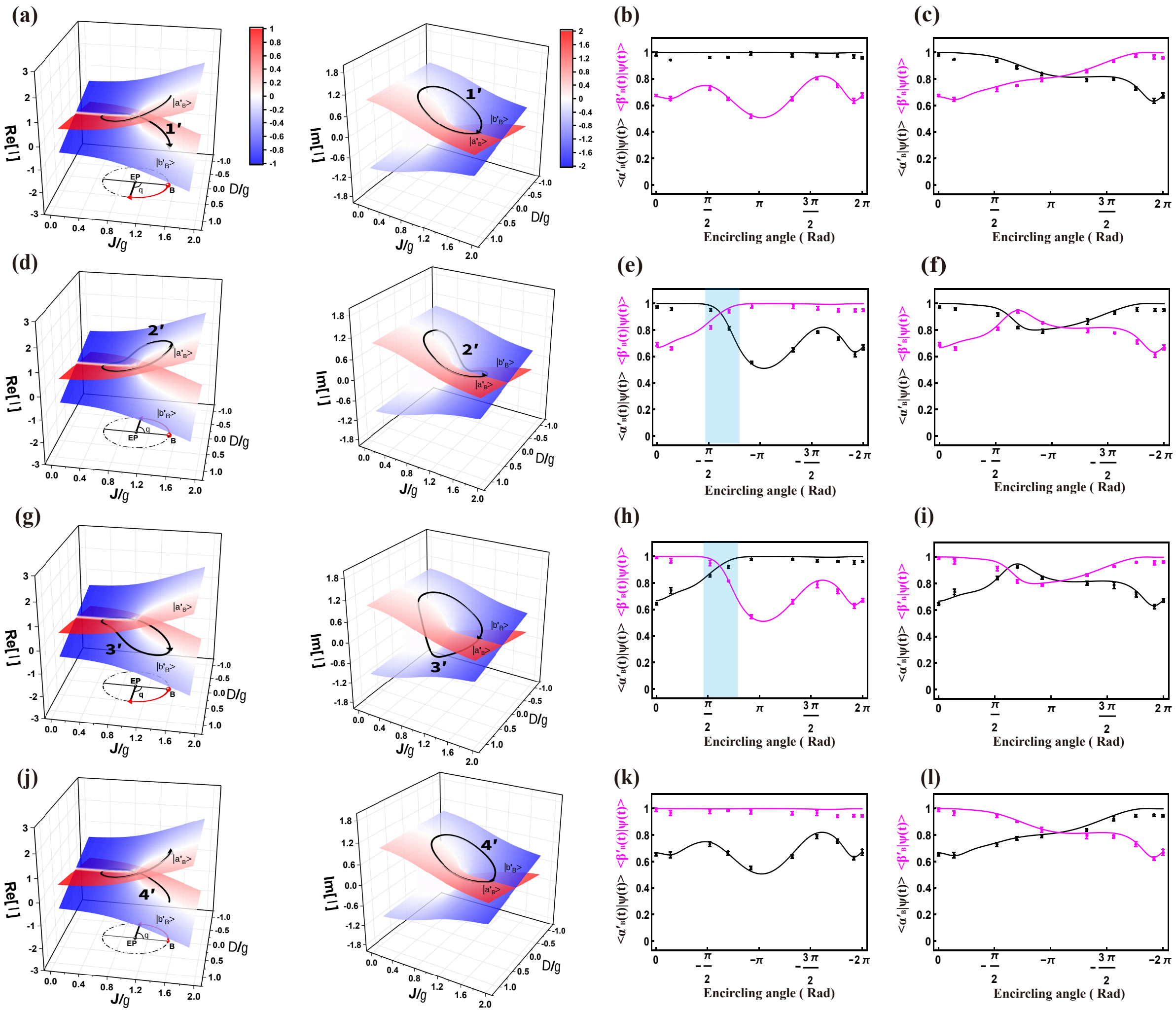

Figure S5: Time evolution of $|\psi(t)\rangle$ starting from the $\mathcal{PTB}$ regime with the $\mathcal{APT}$ symmetric Hamiltonian. The first two columns (a, d, g, and j) depict the trajectories of the state evolution on the eigenvalue Riemann surface. The third column (b, e, h, and k) depicts the overlap between the evolutionary state and two time-dependent eigenstates $\langle\alpha'_B(t)|\psi(t)\rangle$ and $\langle\beta'_B(t)|\psi(t)\rangle$, where the cyan shaded regions indicate the occurrence of non-adiabatic dynamics. The fourth column (c, f, i, and l) represents the overlap between the evolutionary state and two initial eigenstates. (a–c) Clockwise encircling with the initial state $|\alpha'_B(0)\rangle$. (d–f) Counterclockwise encircling with the initial state $|\alpha'_B(0)\rangle$. (g–i) Clockwise encircling with the initial state $|\beta'_B(0)\rangle$. (j–l) Counterclockwise encircling with the initial state $|\beta'_B(0)\rangle$. Circles and lines represent experimental measurements and numerical simulations, respectively.

The DNATs with the $\mathcal{APT}$-symmetric Hamiltonian have also been measured in our experiments. In this context, the nonadiabatic transition amplitudes for the $\mathcal{APT}$-symmetric Hamiltonian can be defined using the same method as that employed for the $\mathcal{PT}$-symmetric Hamiltonian.

$$\begin{aligned} \dot{R}_1'(t) &= -2i\lambda R_1'(t) - if'(1+(R_1'(t))^2) \\ \dot{R}_2'(t) &= 2i\lambda R_2'(t) + if'(1+(R_2'(t))^2), \end{aligned} \tag{S4}$$

where

$$f' = \frac{\dot{J}(i\gamma+\Delta/2) - J(i\dot{\gamma}+\dot{\Delta}/2)}{2i\lambda^2}. \tag{S5}$$

The time-varying relative nonadiabatic transition amplitude $R_1'(t) = \frac{C_2'(t)}{C_1'(t)}$ and $R_2'(t) = \frac{C_1'(t)}{C_2'(t)}$ can also be obtained by numerically solving Eq. S4.

Table S1: Chiral, nonchiral, reciprocal, and nonreciprocal dynamic behaviors in a dissipative quantum system.

	Chirality	Nonchirality	Reciprocity	Nonreciprocity
$[\mathcal{PT}, H] = 0$	Trajectories 1 and 2		1 and 4	2 and 1
$\mathcal{PT}\lvert\psi\rangle = \lvert\psi\rangle$	Trajectories 3 and 4		4 and 1	3 and 4
$\{\mathcal{PT}, H\} = 0$	$1'$ and $2'$		$1'$ and $4'$	$2'$ and $1'$
$\mathcal{PT}\lvert\psi\rangle \neq \lvert\psi\rangle$	$3'$ and $4'$		$4'$ and $1'$	$3'$ and $4'$
$[\mathcal{PT}, H] = 0$		5 and 6	5 and 6	7 and 6
$\mathcal{PT}\lvert\psi\rangle \neq \lvert\psi\rangle$		7 and 8	6 and 5	8 and 5
$\{\mathcal{PT}, H\} = 0$		$5'$ and $6'$	$5'$ and $6'$	$7'$ and $6'$
$\mathcal{PT}\lvert\psi\rangle = \lvert\psi\rangle$		$7'$ and $8'$	$6'$ and $5'$	$8'$ and $5'$

Furthermore, we investigate the adiabatic theorem for dynamical encircling of the EP with the $\mathcal{APT}$-symmetric Hamiltonian. The details are presented in the Figs. S8 and S9. These observations are quite similar to those with the $\mathcal{PT}$-symmetric Hamiltonian, as expected since they share the same Riemann surface of the eigenvalues.

The results with the initial states of $|\beta_A'(0)\rangle$ (in the $\mathcal{PTS}$ regime) and $|\beta_B'(0)\rangle$ (in the $\mathcal{PTB}$ regime) are shown in Fig. S10 (a to b) and Fig. S10 (c to d), respectively. In both cases, the

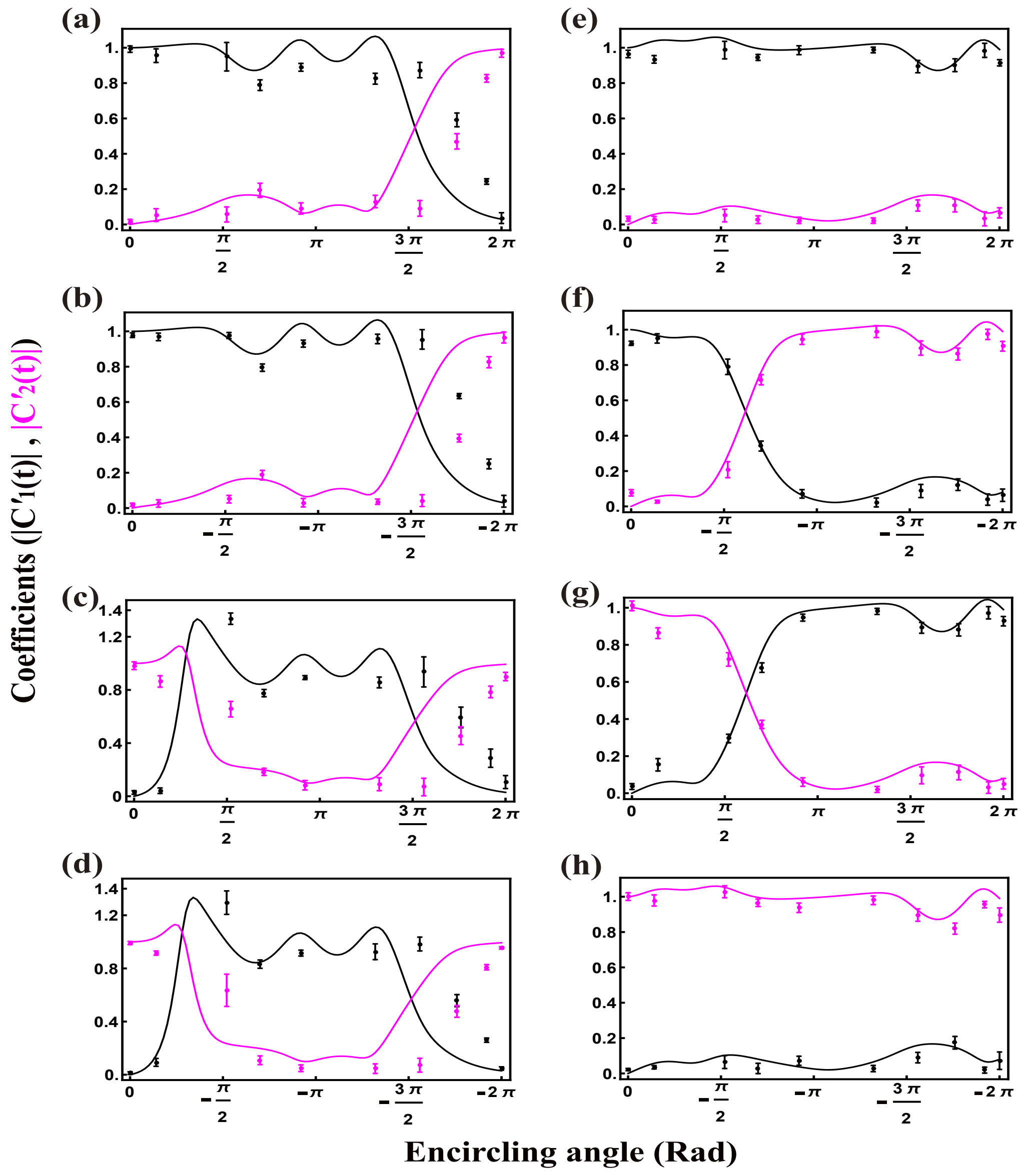

Figure S6: Amplitude coefficients of the instantaneous eigenstates when the $\mathcal{APT}$ Hamiltonian encircles the EP. (a-d) Encircling starting from the $\mathcal{PT}$ symmetric regime: (a) Clockwise with the initial state $|\alpha'_A(0)\rangle$. (b) Counterclockwise with the initial state $|\alpha'_A(0)\rangle$. (c) Clockwise with the initial state $|\beta'_A(0)\rangle$. (d) Counterclockwise with the initial state $|\beta'_A(0)\rangle$. (e-h) Encircling starting from the $\mathcal{PT}$ broken regime: (e) Clockwise with the initial state $|\alpha'_B(0)\rangle$. (f) Counterclockwise with the initial state $|\alpha'_B(0)\rangle$. (g) Clockwise with the initial state $|\beta'_B(0)\rangle$. (h) Counterclockwise with the initial state $|\beta'_B(0)\rangle$. Amplitude coefficients of $C'_1(t)$ and $C'_2(t)$ are similarly determined by $|\psi(t)\rangle = C'_1(t)|\alpha'(t)\rangle + C'_2(t)|\beta'(t)\rangle$.

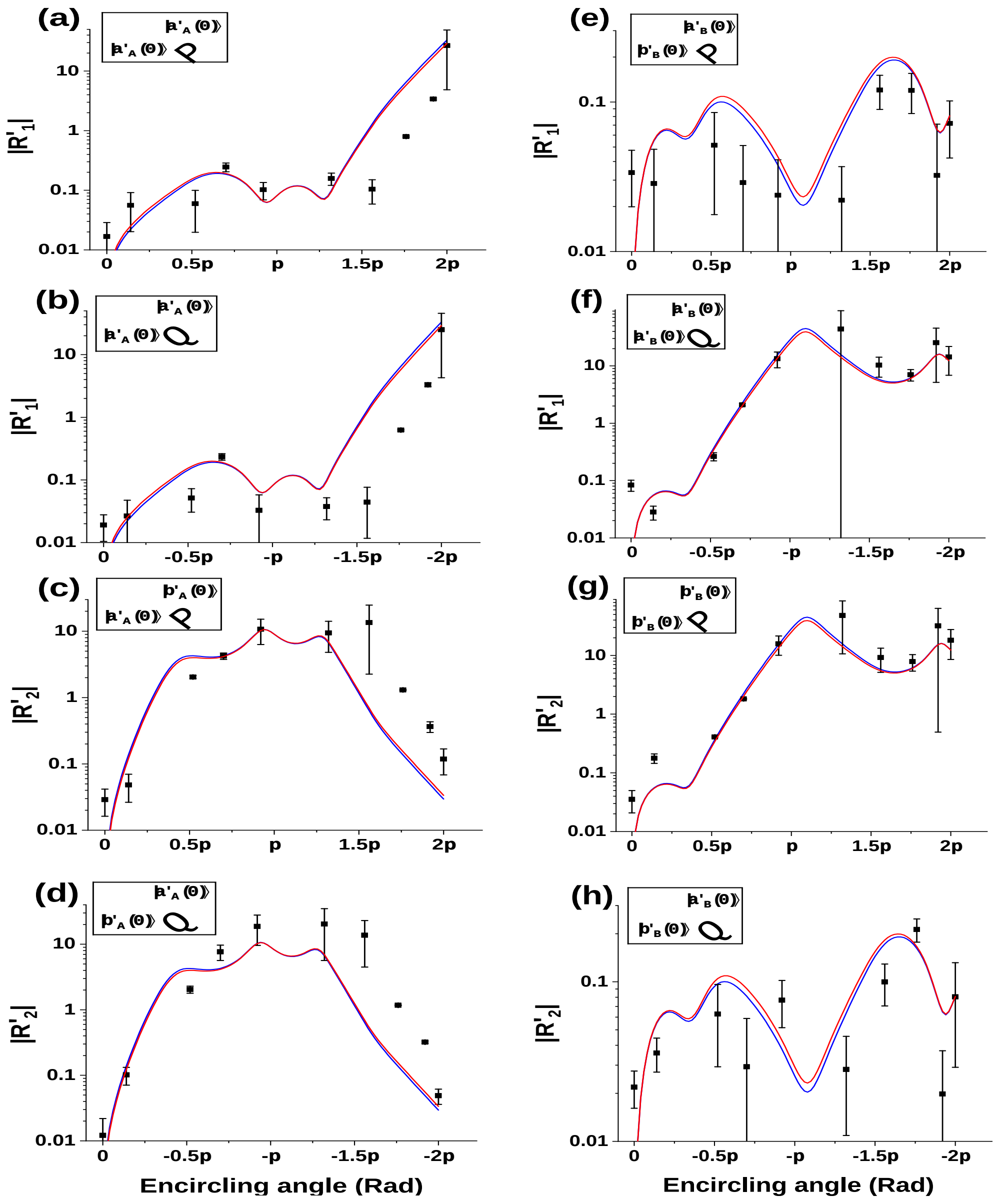

Figure S7: The time-dependent nonadiabatic transition amplitude when the $\mathcal{APT}$ Hamiltonian encircles the EP. (a-d) Encircling starting from the $\mathcal{PT}$ symmetric regime, with (a) Clockwise with the initial state $|\alpha'_A(0)\rangle$, (b) Counterclockwise with the initial state $|\alpha'_A(0)\rangle$, (c) Clockwise with the initial state $|\beta'_A(0)\rangle$, (d) Counterclockwise with the initial state $|\beta'_A(0)\rangle$. (e-h) Encircling starting from the $\mathcal{PT}$ broken regime, with (e) Clockwise with the initial state $|\alpha'_B(0)\rangle$, (f) Counterclockwise with the initial state $|\alpha'_B(0)\rangle$, (g) Clockwise with the initial state $|\beta'_B(0)\rangle$, (h) Counterclockwise with the initial state $|\beta'_B(0)\rangle$. The black squares with error bars represent experimental data. Red and blues lines correspond to theoretical calculations from Eq. S4 and numerical simulations from $C'_1(t)$ and $C'_2(t)$.

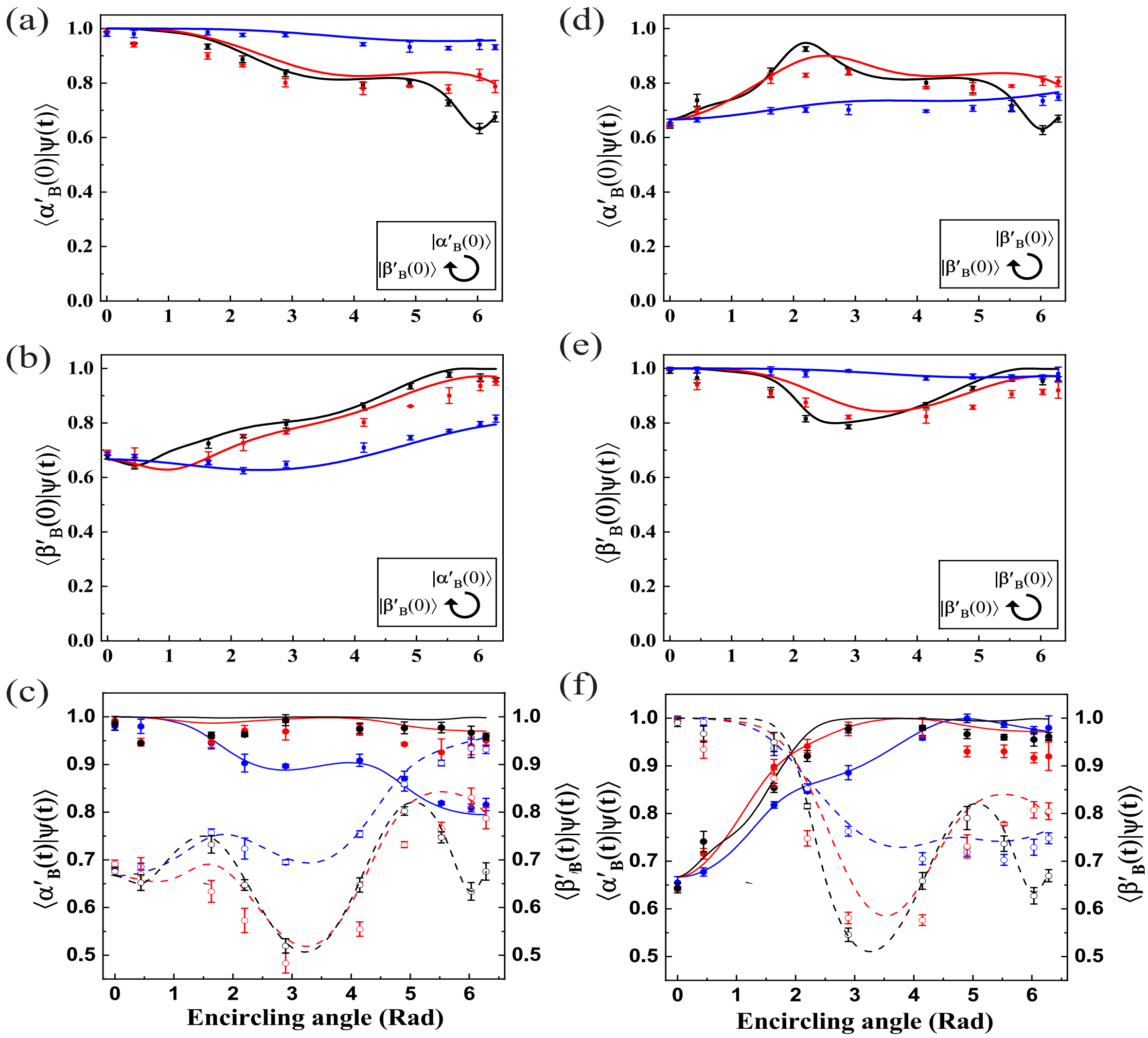

Figure S8: The encircling of the EP of the $\mathcal{APT}$ Hamiltonian with various periods. (a-c) Clockwise encircling the EP with the initial eigenstate $|\alpha'_B(0)\rangle$. (a) and (b) are $\langle\alpha'_B(0)|\psi(t)\rangle$ and $\langle\beta'_B(0)|\psi(t)\rangle$, respectively. (c) $\langle\alpha'_B(t)|\psi(t)\rangle$ (solid line) and $\langle\beta'_B(t)|\psi(t)\rangle$ (dash line). (d-f) Clockwise encircling the EP with the initial eigenstate $|\beta'_B(0)\rangle$, where the notation in (d-f) are the same as (a-c). The blue, red, and black circles correspond to $T = 16.67\ \mu s$, $100\ \mu s$, and $250\ \mu s$, respectively. The lines represent the numerical simulations.

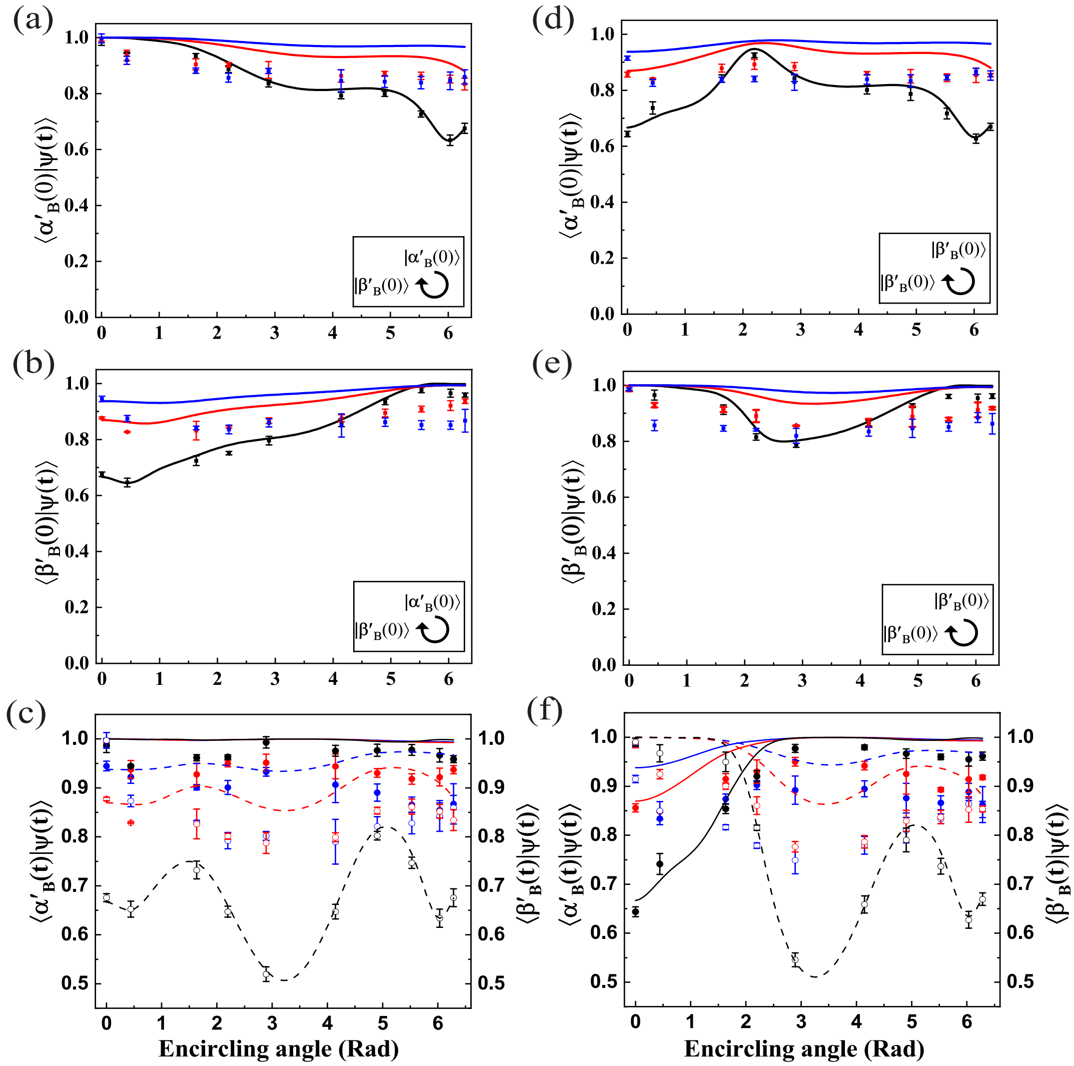

Figure S9: The encircling of the EP of the $\mathcal{APT}$ Hamiltonian with various radii. The notation for (a-f) is similar to Fig. S8 (a-f) as defined previously. The blue, red, and black squares correspond to r =0.004 MHz, 0.009 MHz, and 0.03 MHz, respectively. The lines represent the numerical simulations.

experimental data match well with the theoretically predicted values despite varying noise intensities, thereby validating the robustness of topological state transfers with the $\mathcal{APT}$-symmetric Hamiltonian.

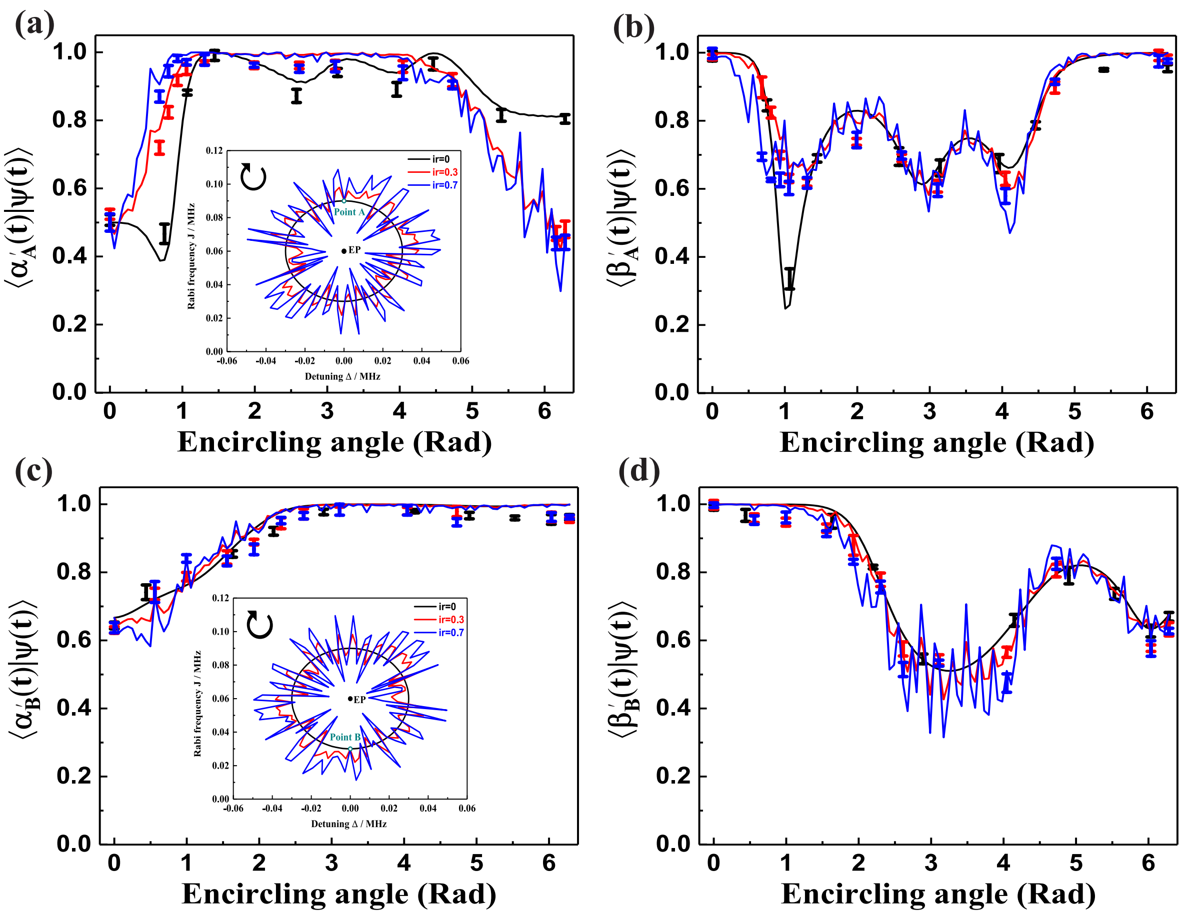

Figure S10: Quantum state transfers while encircling the EP of the $\mathcal{APT}$ Hamiltonian with various noise intensities. (a-b) The clockwise encircling from the initial state $|\beta'_A(0)\rangle$. (c-d) The clockwise encircling from the initial state $|\beta'_B(0)\rangle$. The insets in (a) and (c) display the encircling trajectories in the parameter space $\{\Delta, J\}$ with random noise intensities $ir = 0$ (black), 0.3 (red), and 0.7 (blue), respectively. The dots are experimental results, while the solid lines represent the numerical simulations.

Supplementary References

1. H. Shen, B. Zhen, L. Fu, Topological band theory for non-Hermitian Hamiltonians. *Physical Review Letters* **120**, 146402 (2018).

2. J. Bian, P.-F. Lu, T. Liu, H. Wu, X.-X. Rao, K.-X. Wang, Q.-F. Lao, Y. Liu, F. Zhu, L. Luo, Quantum simulation of a general anti-PT-symmetric Hamiltonian with a trapped ion qubit. *Fundamental Research* **3**, 904-908 (2023).

3. F. Zhang, Y. Feng, X. Chen, L. Ge, W. W, Synthetic Anti-PT Symmetry in a Single Microcavity. *Physical Review Letters* **124**, 053901 (2020).